

# Recent ice dynamic and surface mass balance of Union Glacier in the West Antarctic Ice Sheet

Andrés Rivera<sup>1,2</sup>, Rodrigo Zamora<sup>1</sup>, José Andrés Uribe<sup>1</sup>, Ricardo Jaña<sup>3</sup>, and Jonathan Oberreuter<sup>1</sup>

<sup>1</sup>Centro de Estudios Científicos, PO Box 5110466, Valdivia, Chile

<sup>2</sup>Departamento de Geografía, Universidad de Chile, PO Box 3387, Santiago, Chile

<sup>3</sup>Instituto Antártico Chileno, Punta Arenas, Chile

*Correspondence to:* Andrés Rivera,  
(arivera@cecs.cl)

**Abstract.** Here we present the results of a comprehensive glaciological investigation of Union Glacier (79°46'S/83°24'W) in the West Antarctic Ice Sheet (WAIS), a major outlet glacier within the Ellsworth Mountains. Union Glacier flows into the Ronne Ice Shelf, where recent models have indicated the potential for significant grounding line zone (GLZ) migrations in response to changing climate and ocean conditions. To elaborate a glaciological base line that can help to evaluate the potential impact of this GLZ change scenario, we installed an array of stakes on Union Glacier in 2007. The stake network has been surveyed repeatedly for elevation, velocity, and net surface mass balance. The region of the stake measurements is in near-equilibrium, and ice speed is 10 to 33 m a<sup>-1</sup>. Ground-penetrating radars (GPR) have been used to map the sub-glacial topography, internal structure, and crevasse frequency and depth along surveyed tracks in the stake site area. The bedrock in this area has a minimum elevation of -858 m a.s.l., significantly deeper than BEDMAP2 data. However, between this deeper area and the local GLZ, there is a threshold where the subglacial topography shows a maximum altitude of 190 m. This subglacial condition implies that an upstream migration of the GLZ will not have strong effects on Union Glacier, until passing beyond this shallow ice pinning point.

underneath WAIS is inversed (ice is deeper upstream) and steeper than at the present grounding line zones (GLZ) (Ross et al., 2012). This topographic condition, in a context of ongoing global changes, especially oceanic warming in areas of the Southern Ocean, is leading to GLZ upstream migration, as observed for example at the Amundsen Sea Embayment Area (ASEA) glaciers, like Pine Island (PIG) and Thwaites (Rignot et al., 2002). This migration process in a context of inversed subglacial topographies, has an impact on glacier dynamics, since bottom melting at the GLZ is higher in deeper waters, provoking higher ice fluxes, ice thinning and, in general, a more negative mass balance (Rignot and Jacobs, 2002). However, there are WAIS areas where the changes are not as dramatic as observed at ASEA, with some regions thickening rather than thinning (Joughin and Bamber, 2005).

One of the WAIS areas where glaciological changes are not strong at present is the Weddell Sea sector (Rignot and Thomas, 2002), where the Ronne Ice Shelf (RnIS) is located (Fig. 1). This floating platform has been relatively stable in recent decades, with different behaviours of the GLZ and very small net mass balance changes (Rignot et al., 2011b). The relative stability of the RnIS is partly explained by the Weddell Seas oceanographic and atmospheric conditions, and the associated broad extent of sea ice (Mayewski et al., 2009). The sea ice extents in this area has been stable (Cavalieri and Parkinson, 2008), but recent studies (Hellmer et al., 2012) forecast a sea ice volume reduction for the XXI century resulting in incremental circulation of warm water beneath the Filchner ice shelf toward the GLZ of the Slessor, Recovery, Support Force, Möller and Foundation ice streams. The intrusion of warmer waters will certainly increase the basal melt rate of the ice shelf, and possibly lead to retreat of

## 1 Introduction

WAIS, the West Antarctic Ice sheet (Fig. 1) has been considered potentially unstable because its bedrock is located well below sea level (Bamber et al., 2009), and its total disintegration could contribute up to 4.3 m (Fretwell et al., 2013) to global sea-level rise. In many cases, the topography

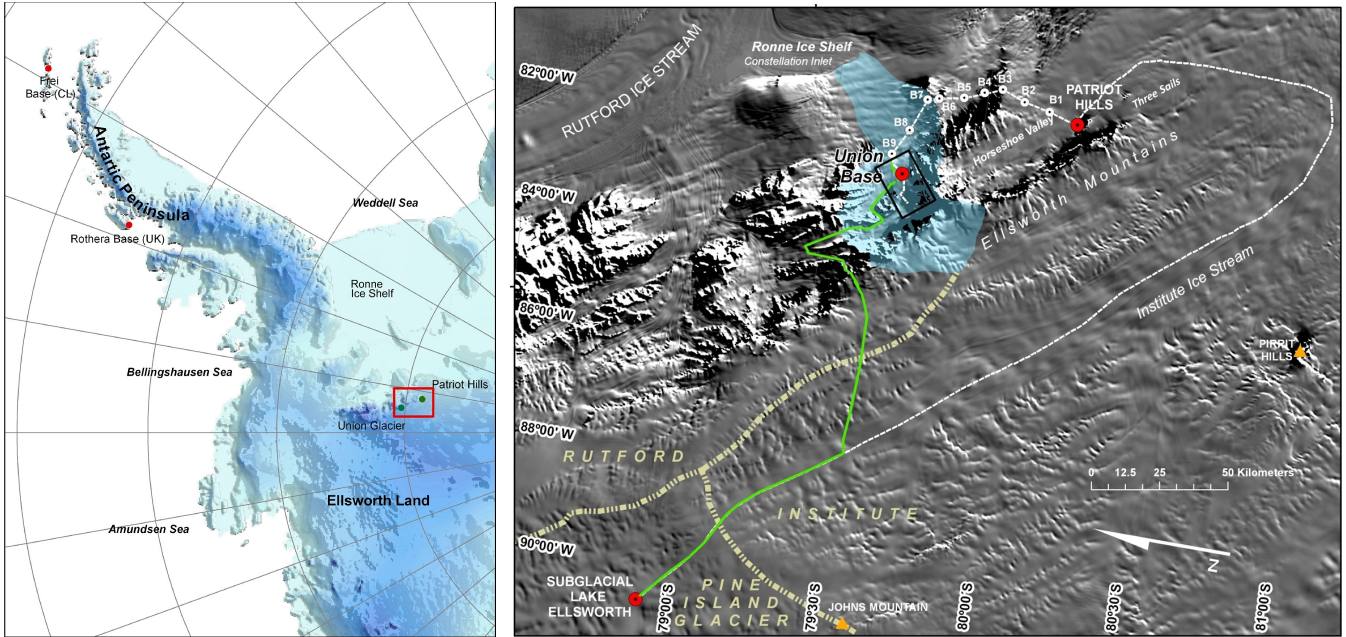


**Figure 1.** Left: WAIS Location map. Right: Union Glacier basin (light blue area). In yellow, the main ice divides in the region. In dashed white the 2005 track to Subglacial Lake Ellsworth (517 km). In green, the new track surveyed in 2010 (235 km). Stakes B1 to B9 are described in the text. The black box is shown in Figure 2. Background image: MODIS Mosaic of Antarctica (MOA: Scambos et al., 2007).

the GLZ. This, in turn, would favour higher ice fluxes along tributary glaciers, and thinning that will spread upstream along deep channels (Rignot et al., 2011b).

Between two of the main ice streams in the region (Rutford and Institute), there are two smaller glaciers also draining into the RnIS; Union Glacier ( $79^{\circ}46'S/83^{\circ}24'W$ ) flowing into the Constellation inlet and the Horseshoe valley Glacier ( $80^{\circ}18'S/81^{\circ}22'W$ ) flowing into the Hercules inlet. The study of these glaciers could provide an important clue about ongoing changes taking place in the region, especially considering that local glacier mass balance can be significantly affected by RnIS changes.

In this context, the main aim of this paper is to present recent glaciological results obtained at the Union Glacier and nearby areas that provide a base line for possible ice dynamic responses to ongoing and modelled future changes of RnIS.

## 2 Study Area

Union Glacier ( $79^{\circ}46'S/83^{\circ}24'W$ ) (Fig. 2) has an estimated total area of  $2561 \text{ km}^2$ , with a total length of 86 km from the ice divide with Institute ice stream down to the grounding line of the Constellation Inlet on the RnIS. The glacier has several glacier tributaries, the main trunks being located in the Union and Schanz valleys (Figs. 1 and 2), which are feed through narrow glacial valleys (9 km wide) flowing from the interior plateau until they merge at the Union “gate”. This

gate or narrowest section of the glacier (7 km wide), has a medial moraine line comprised of clasts and small-sized debris.

The local Union Glacier BIA is used for landing Ilyushin IL76 airplanes on wheels under a contract with the private company Antarctic Logistics and Expeditions (ALE) llc. This company has been operating in the region since the 1980s, when they began to use the Patriot Hills BIA (Wendt et al., 2009) at the Horseshoe Valley ( $80^{\circ}18'S/81^{\circ}22'W$ ) for landing heavy airplanes. However, these airplane operations were frequently disrupted due to strong prevailing cross winds at Patriot Hills. In order to increase the number of airplane operational days and improve access for heavy cargo airplanes, in 2007/8 ALE moved to Union Glacier, where the prevailing wind direction is in line with the landing strip (katabatic winds), helping airplanes to operate even with strong gusts. Thanks to ALE logistic support, four scientific campaigns have been conducted on Union Glacier since 2008, where a glaciological program was established, including ice dynamic, mass balance and geophysical surveys (Rivera et al., 2010).

An array of 21 stakes was installed at the gate in 2007 for ice dynamic and surface mass balance studies. The Union gate has been re-surveyed by using GPS and radar systems installed onboard convoys pulled by Camoplast tractors travelling along pre designated routes. Results of the first campaigns of 2007 and 2008 were published by Rivera et al. (2010).

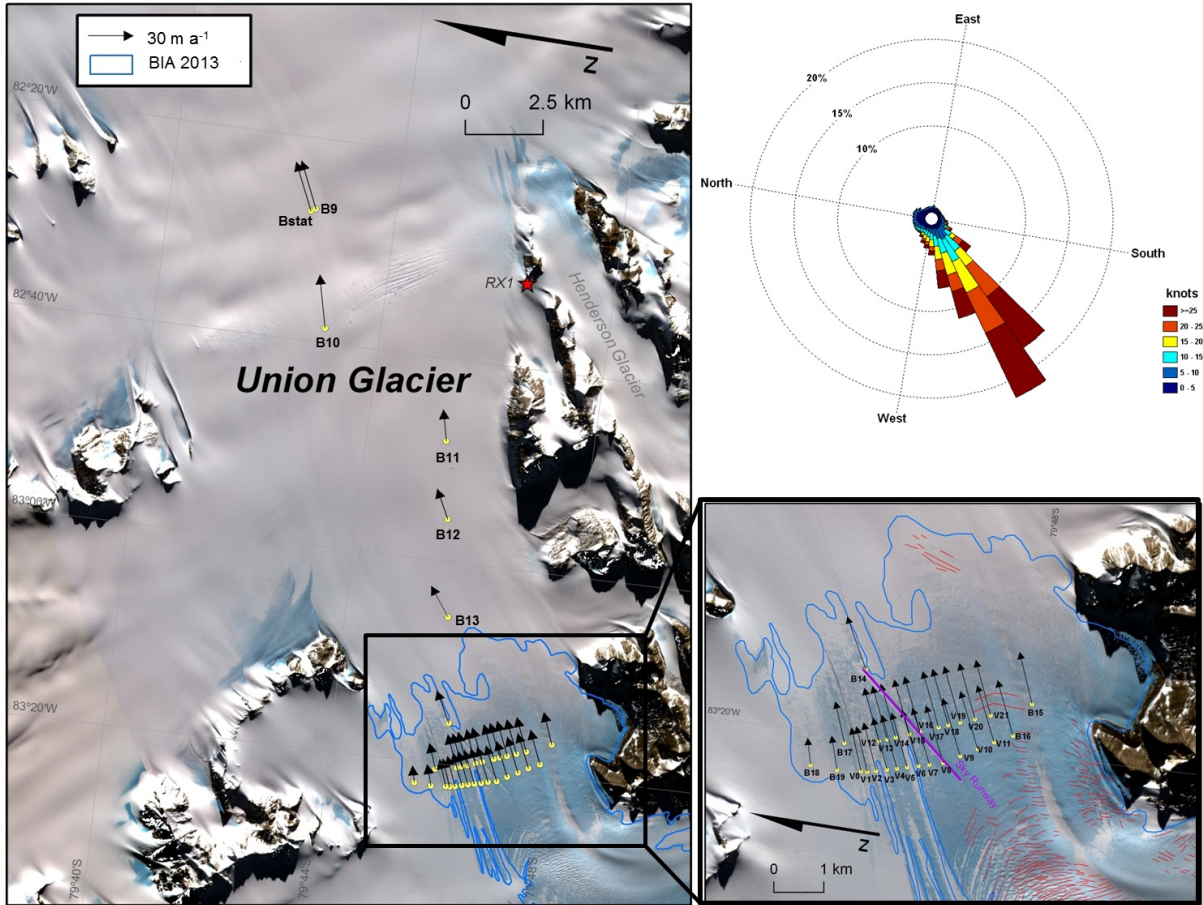


**Figure 2.** Yellow dots show the stakes described in the text (Fig. 1 and Table 2). RX1 is the location of the static GPS on rock. Crevasse are shown in red. The Union Glacier “gate” is a transversal profile between B18 and B15 (inset) where the ice runway is shown in purple. Mean ice velocities area shown as arrows. Summer base camp is visible near B11. The background image is an ASTER false composite 321 acquired on 1 February 2013. Upper right: Predominant wind speed and direction 2008-2012 at the Union Glacier Automatic Weather Station, installed near stake V17.

### 3 Methods

#### 3.1 Meteorological data

The meteorological data analysed here was collected at the 135  
 Union Glacier Automatic Weather Station (AWS) installed near stake V17, which has been operating since 2008 (Fig. 2). The AWS data series show several data gaps due to malfunction or low power supply problems during the winter. In spite of these, the available data are good enough for 140  
 weather forecast during landing operations in the summer, and for describing general temperature conditions in the area, as well as predominant winds and directions. 145

#### 3.2 Remote sensing

Mid-summer ASTER satellite images acquired between 130  
 2002 and 2013 (Table 1) were analyzed and classified via

manual digitalization in order to delineate the local Union Glacier main BIA. This task allowed areal changes in snow cover to be quantified and analysed for possible relationships with local meteorological data.

The ASTER images were geometrically corrected using the internal parameters of each scene. A true colour composition (Band 1, 2 and 3N) for each year was produced and the contrast and brightness modified by the means of histogram equalization to facilitate the delimitation of the blue ice area.

The BIA outline mapping was based upon a similar procedure established by Rivera et al. (2014), where the boundary between snow and ice is manually identified assuming the maximum extent criterion of identification. This is easily done thanks to the spectral differences between snow and ice.

### 3.3 Glaciological mass balance

Stake heights above the snow/ice surface were measured yearly between 2007 and 2011 (Figs. 1 and 2: Table 2). Of 88 potential stake measurements at the gate, 72 were successfully acquired. The annual heights were compared and local mass balance was subsequently calculated. In order to convert these values into water equivalent, a mean density of 910 kg m<sup>-3</sup> (Paterson, 1994) was used for stakes drilled on ice. In those cases where the stakes were located at snow surfaces, the densities were measured by using a Mount Rose snow probe with penetration capacity of near 50 cm of snow-firn. The snow density accuracy obtained by the use of this device is estimated to be near 12% (Conger and McClung, 2009).

### 3.4 GPS

In December 2007, the initial observation network of 21 bamboo-stakes was installed on a blue ice area (BIA) on the Union Glacier (Fig. 2). For each of these stakes GPS measurements were made using Topcon GR3 dual frequency GPS receivers with measurement times of less than 30 s per stake, yielding metre scale errors. In December 2008, 2009 and 2010, the same network, as well as 35 new stakes were surveyed with dual frequency Javad GPS model Lexon GGD receivers. In order to apply a differential correction procedure, a similar GPS receiver was continuously collecting data at a rock location (RX1 in Fig. 2). The precision obtained by these surveys improved to less than 10 cm, by measuring between 15-30 minutes per stake. Additionally, a dual frequency Javad GPS receiver was installed on snow (Bstat in Fig. 2) collecting data between 11 December 2009 and 31 January 2010 for high resolution studies (each 30 s), with the aim of detecting possible tidal modulated ice velocities. In January 2011, a Real Time Kinematic procedure was applied to data collected at the Union Glacier gate by a Leica SR 9500 receiver, with estimated decimetre accuracy. All GPS data collected were processed using the commercial software GrafNav 8.20.

### 3.5 Surface elevation changes and geodetic mass balance estimation

The data obtained by the GPS measurements were compared in order to calculate the local mass balance and the absolute surface elevation changes at the BIA.

Using the measured height differences obtained by GPS and considering the surface topographic slope effect, the submergence/emergence velocity ( $w_e$ ) was calculated:

$$w_e = w_s - u_s \tan \alpha \quad (1)$$

where  $w_s$  is the vertical ice velocity,  $u_s$  is the ice velocity along the surface flow direction and  $\alpha$  is the slope. The

emergence velocity represents the vertical flow of ice relative to the glaciers surface and allows the estimation of the net balance if it is assumed that density does not change with depth during the period (Hooke, 2005).

By subtracting the emergence velocity of the measured specific balance (stake height difference) the surface elevation change with time at a fixed position can be obtained.

$$\frac{\partial h}{\partial t} = b - w_e \quad (2)$$

If the glacier is in a steady state, there would be no surface changes since accumulation and ablation compensates for the submergence and emergence velocities so that the surface profile remains unchanged (Hooke, 2005). In this case  $b = w_e$ , however most glaciers are not perfectly in steady state. Only the stake array measured at the Union gate was considered for this analysis.

### 3.6 Radar

A coherent pulse compression radar depth sounder designed at CECs (Uribe et al., 2014) was used to measure ice thickness. The radar operates at a central frequency of 155 MHz, a maximum of 10 kHz of pulse repetition frequency (PRF), a bandwidth of 20 MHz and 200 W of peak power. Yagi antennae were used for both the transmitter and receiver. We use two channels for simultaneous low and high signal amplification to increase the dynamic range of this radar.

A Frequency Modulated - Continuous Wave (FM-CW) radar also designed by Uribe et al. (2014), was used to measure surface snow and ice layering to a depth of 450 m with high vertical resolution (1 m). This radar works at a frequency from 550 MHz to 900 MHz using two separated log periodic antennae for the transmitter and receiver. The transmit power was 21 dBm, and the whole system operated at a PRF of 10 kHz. A Direct Digital Synthesis (DDS) system was used to generate an extremely linear frequency sweep transmitted signal.

The third radar system used along these tracks was a commercial Ground Penetrating Radar (GPR), a Geophysical Survey Systems Inc. (GSSI) model SIR-3000, working at 400 MHz. The range was set between 190 and 300 ns to record subsurface reflection with the aim to find crevasses in real time. The GPR antennae were mounted on a 7 m long rod which was attached to a tractor and had rubber car tyre tube installed at the opposite end. The radar data were analysed in real time while the tractor was moving, in order to alert the driver of the presence of hyperbolae, potentially related to crevasses.

Post processing and data analyses were carried out using Reflex-Win V5.6 (Sandmeier Scientific Software) for the three radar systems. A background removal, dewow

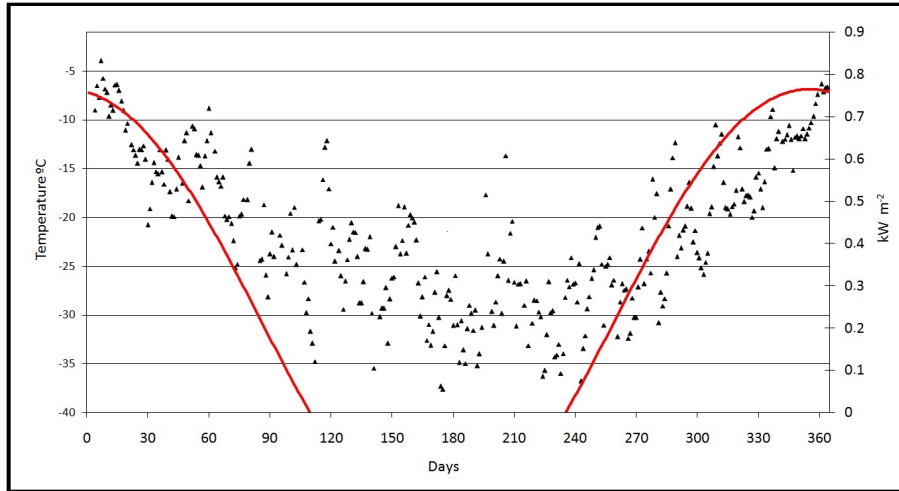


**Figure 3.** Mean daily temperature ( $^{\circ}\text{C}$ ) during 2008 (black triangles) and modeled solar direct radiation (red line) at the AWS site ( $\text{kW m}^{-2}$ ).

245 filter and adjustment of the gain function, among others  
 246 procedures, were applied to the raw data. For crevasses  
 247 analysis, migration correction procedures were also applied  
 248 to collapse the hyperbolic diffractions to their proper point  
 249 origins (Plewes and Hubbard, 2001). In order to convert  
 250 travel time to ice thickness in metres, it was assumed that  
 251 the electromagnetic wave travelled through the ice at 0.168  
 252  $\text{m ns}^{-1}$ , a mean value representative of cold ice (Glen  
 253 and Paren, 1975) and at 0.194  $\text{m ns}^{-1}$  assumed to be  
 254 representative for snow/firm (Woodward and King, 2009).

255 **4 Results**

**4.1 Meteorological data and BIA area changes**

260 The meteorological data collected at Union Glacier between  
 261 2008 and 2013 contains several gaps and non valid records,  
 262 but in general provide a good idea of the local conditions,  
 263 which are especially useful for landing operations. In terms  
 264 of climatological analysis, the series is too short and noisy,  
 265 but is the only one available in the region.

266 The mean daily air temperature at this location (Fig. 3)  
 267 from 2008 to 2012 was  $-20.6^{\circ}\text{C}$ , with an absolute minimum  
 268 of  $-42.7^{\circ}\text{C}$  recorded on 12 August 2008 at 2 a.m. and  
 269 an absolute maximum of  $0.5^{\circ}\text{C}$  registered on 15 January  
 270 2010 at 8 p.m. Daily air temperatures have maximums in  
 271 December-January following direct solar radiation, however  
 272 between April and August (included) when the Sun is below  
 273 the horizon, the lowest temperatures have a mean of  
 274  $-25.5 \pm 3.5^{\circ}\text{C}$ . Temperatures close to the melting point have  
 275 only been observed in three summer events: 7-8 January 2008,  
 276 14-15 January 2010 and 25-26 December 2010, but no

surface melting has been observed on this site. The mean air  
 277 temperature in January is  $-10.3^{\circ}\text{C}$ .

278 Regarding wind speed and direction, the data are  
 279 very consistent between 2008-2012 with a mean value  
 280 16.3 knots and predominant direction from  $224^{\circ}$ . The  
 281 maximum wind speed recorded on site was near 60 knots  
 282 and the predominant wind speeds are higher than 25  
 283 knots (Fig. 2). This predominant wind direction explains  
 284 the extension of the main BIA which has experienced  
 285 less than 10% area changes between 2002 and 2013.  
 The available scene dates are showing some expected  
 286 seasonally variability, especially when comparing more  
 287 stable midsummer (December-January) with early or late  
 288 summer scenes (Brown and Scambos, 2005). The series is  
 289 however too short to detect a trend (Table 1).

**4.2 Surface mass balance**

290 Snow densities measured at stakes drilled on snow surfaces  
 291 have a mean value of  $400 \pm 3 \text{ kg m}^{-3}$ , with small variability  
 292 between all surveyed stakes. No fresh and soft snow was  
 293 detected due to the lack of precipitation in the region during  
 294 our surveys. Table 2 indicates the details of each stake, the  
 295 type of surface and period of measurements.

296 The surface mass balance estimations between 2007 and  
 297 2011 at the stakes installed on the BIA gate (V00 to V21,  
 298 Table 2), are typically negative (Fig. 4), with a mean inter  
 299 annual surface mass balance of  $-0.097 \text{ m w.eq. a}^{-1}$ .

300 The stakes installed along the traverse between Patriot  
 301 Hills and Union Glacier (Fig. 1) were only measured between  
 302 2008 and 2009 and showed differing results depending on  
 303 their location. Stakes installed on snow surfaces (B1-B12)  
 304 have positive mass balances with a mean snow accumulation  
 305 of  $0.3 \text{ m a}^{-1}$  ( $0.12 \text{ m w.eq. a}^{-1}$ ). Just outside the BIA, stake

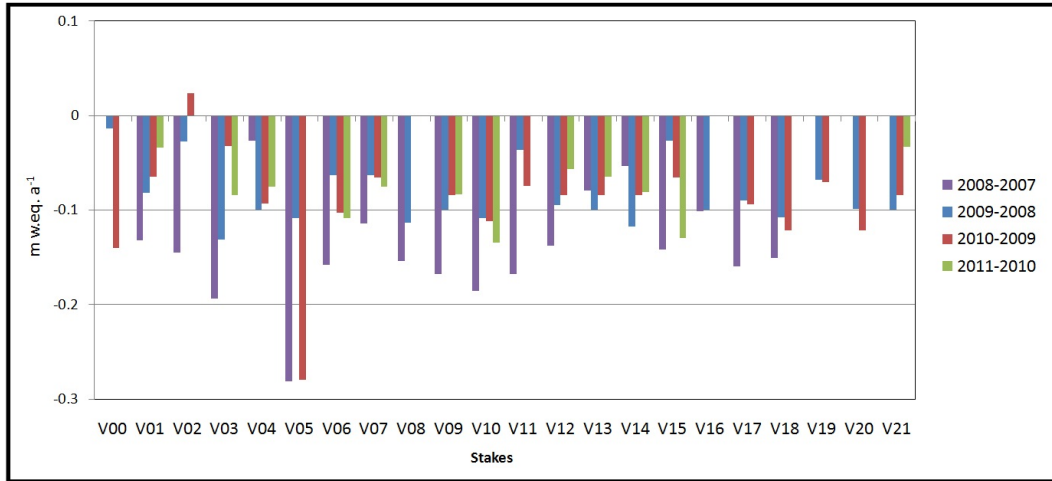


Figure 4. Mass balance ( $m \text{ w.eq. a}^{-1}$ ) 2007-2011 at stake located at the local BIA. Stakes locations are shown in Figure 2.

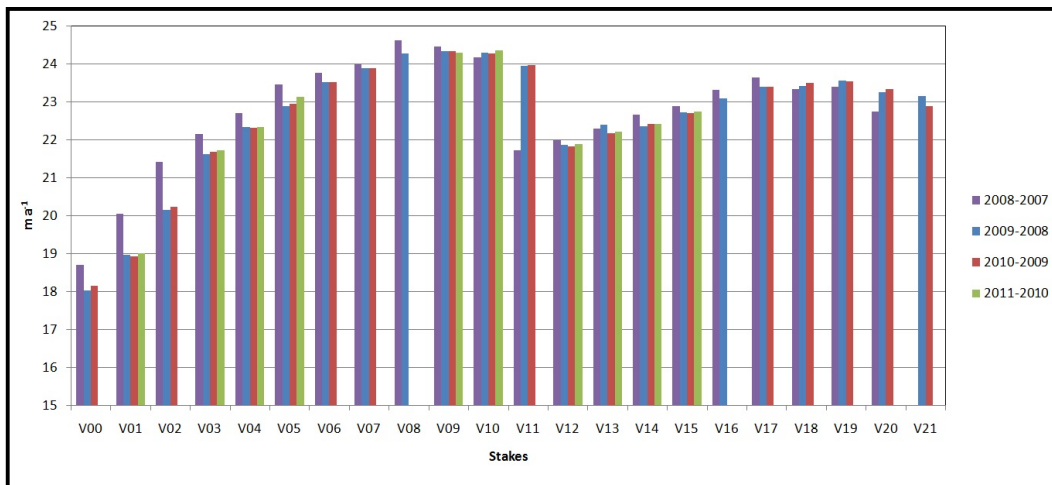


Figure 5. Ice velocities ( $m \text{ a}^{-1}$ ) at the Union Glacier gate by indicated years. Stakes locations are shown in Figure 2.

B12 showed the maximum net balance ( $0.2 \text{ m w.eq. a}^{-1}$ ), indicating that snow drift coming from the BIA, due to the predominant katabatic wind direction (Fig. 2) is having a positive downstream accumulation effect. The only negative surface mass balance along the track Patriot Hills-Union Glacier (excluding the Union Glacier BIA) was detected at stake B5, which is located at the edge of the local BIA of the Plumber glacier (Fig. 1). Here a modest  $-0.07 \text{ m w.eq. a}^{-1}$  (Table 2) was obtained between 2008 and 2009. Stakes B13-B19 (Table 2, Fig. 2), also had negative values with a mean surface balance of  $0.1 \text{ m w.eq. a}^{-1}$ , coincident with the other stakes located at a local BIA.

### 4.3 Surface ice velocity

Surface ice velocities were obtained for 19 stakes (B1-B19) located along the track between Patriot Hills and Union Glacier base camp (Figs. 1 and 2), with measurements periods of near 1 yr, and resulting ice velocities between  $0.1$  and  $34.6 \text{ m a}^{-1}$  (Table 2). Minimum values were observed at local ice divides (B2-B8) while the maximum velocity was observed at stake B10 located at the steepest area of Union Glacier, between two crevasse fields (Fig. 2).

Between 11 December 2009 and 31 January 2010 a dual frequency GPS receiver was attached to stake Bstat, taking continuous measurements every 15 s. The receiver was powered by batteries and solar panels, providing a detailed record of daily ice dynamic during the spanned period of

310

315

330

time. The main aim of this survey was to test the hypothesis that the ice dynamics of Union Glacier are affected by Ronne Ice Shelf tides, as has been observed at the Rutford ice stream 385 where a modulated ice flow was detected (Gudmundsson, 2006). This stake (Bstat, Table 2) is located 38 km upstream of the local grounding line zone of the Constellation inlet at the Ronne Ice Shelf (Figs. 1 and 2). The resulting ice velocity was  $33 \text{ m a}^{-1}$ , and thanks to the analysis carried out by 390 H. Gudmundsson (personal communication, 2010), no tidal effect was detected.

The neighbouring stake to Bstat (B9, located within a distance of 10 m) was only measured for 30 minutes in December 2009 and in December 2010, resulting in 395 an annual velocity of  $33.26 \pm 0.7 \text{ m a}^{-1}$ . The good correspondence with the Bstat results ( $33 \text{ m a}^{-1}$ ) indicates that Union Glacier does not show important seasonal ice velocity changes.

At the Union Glacier gate stake array (Fig. 2), 22 stakes 400 were drilled into its Blue ice Area in 2007 and have been annually resurveyed up until 2011. Unfortunately, not all the original stakes have survived, or were re-measured every year. However, from the remaining stake network a mean velocity of  $20 \text{ m a}^{-1}$  was estimated for the measurement 405 period (Fig. 5). The overall ice motion at the gate is similar to the main wind direction (Fig. 2) observed at the BIA. No temporal velocity changes were observed during the studied period.

#### 4.4 Surface elevation change

360 Considering the surface velocities obtained for the stakes (Table 2) and by applying Eq. 1, a mean vertical velocity for the blue ice of  $-0.07 \pm 0.007 \text{ m a}^{-1}$  was found at the 415 Union Gate. For a steady state glacier this would be equal to the local mass balance however this is not the case for the 365 studied area (there is a negative mass balance at the BIA) and a mean local elevation change of  $-0.012 \text{ m a}^{-1}$  was found. In any case, this result is close to the estimated error of the 420 measurements and indicates near equilibrium conditions.

#### 4.5 Glacier thickness and internal structure

370 More than 450 km of radar tracks were measured between 425 2008 and 2010 at the Union Glacier area, including oversnow traverses between Patriot Hills, Union Glacier and the high Antarctic plateau.

The 80 km long profile between the Antarctic Plateau and Union Glacier (Fig. 6 upper), including the transit 430 along Balish, Schneider, Schanz and Driscoll glaciers, was surveyed with a FM-CW radar for snow accumulation data, a compression pulse radar for ice thickness data and a GPR system for crevasse detection purposes.

380 The deep ice of the plateau is seen at the beginning of the survey profile (A in Fig. 6), then is followed by a passage characterized by shallow ice (B) where the steepest section

of the whole traverse was crossed. After this section, the thickness increases sharply until a local maximum thickness of 1120 m was observed at Balish Glacier. The local divide between the Balish and Schneider glaciers (C in Fig. 6) has a prominent subglacial peak (C in Fig. 6) where the mountain range dividing the two glaciers is also visible underneath the ice. The maximum thickness measured at Schneider Glacier was 900 m, 1050 m at Schanz Glacier, 1510 m in Driscoll Glacier and 1540 m in Union Glacier, close to the base camp. The mean ice thickness measured at Union Glacier was 1450 m. The subglacial topography in the valley is smooth, with “U” shape flanks.

At the beginning of the radar profile (A-B in Fig. 6), it is possible to see the shallowest ice at the Gifford Peaks pass (passage), with a thickness between 45 and 140 m obtained by the low gain channel of the pulse compression radar. This profile is not visible in the high-gain channel, due to set up constrains of this system (Uribe et al., 2014).

The FM-CW radar detected multiple internal snow-firn layers and the snow-ice boundary layer with a high resolution. Figure 7 shows a FM-CW profile at Union Glacier, where the snow/ice boundary layer is at a deep of 30-40 m (between A and B in Fig. 7), and then tends to disappear when approaching the BIA (between C and D in Fig. 7). The central moraine line of the glacier is indicated by letter C in Figure 7.

The GPR data collected along the track from Union 410 Glacier to the Antarctic Plateau allowed the detection of many crevasses both near the runway area, and at the Gifford Peaks passage, just before reaching the plateau. Along the survey route the GPR system was able to detect the upper 20 m of the internal structure of the ice. Within this upper layer annual snow/firn layers suffered (in places) discontinuities due to crevasses that appeared as hyperbolae on the radar traces.

In general, the route from Union Glacier to the Antarctic plateau is almost totally free of crevasses. An exception to this was the Gifford passage (B in Fig. 6) where a minor system of crevasses was detected, with widths between 1 and 5 m, and snow bridges between 1.5 and 3 m thick. In spite of these crevasses, the Gifford passage is the shortest (235 km) gateway for oversnow traverses from Union Glacier to the Subglacial Lake Ellsworth (Vaughan et al., 2007) at the Antarctic plateau. The alternative route to this subglacial lake is near 520 km long, starting at Union Glacier, passing along Patriot Hills, then travelling around the Three Sails and finally turning west toward the Subglacial Lake Ellsworth (Fig. 1).

## 5 Discussion

At Union Glacier, the local BIA is shaped by strong snowdrift caused by katabatic winds accelerated by the slope at the main junction between the two glacial valley arms

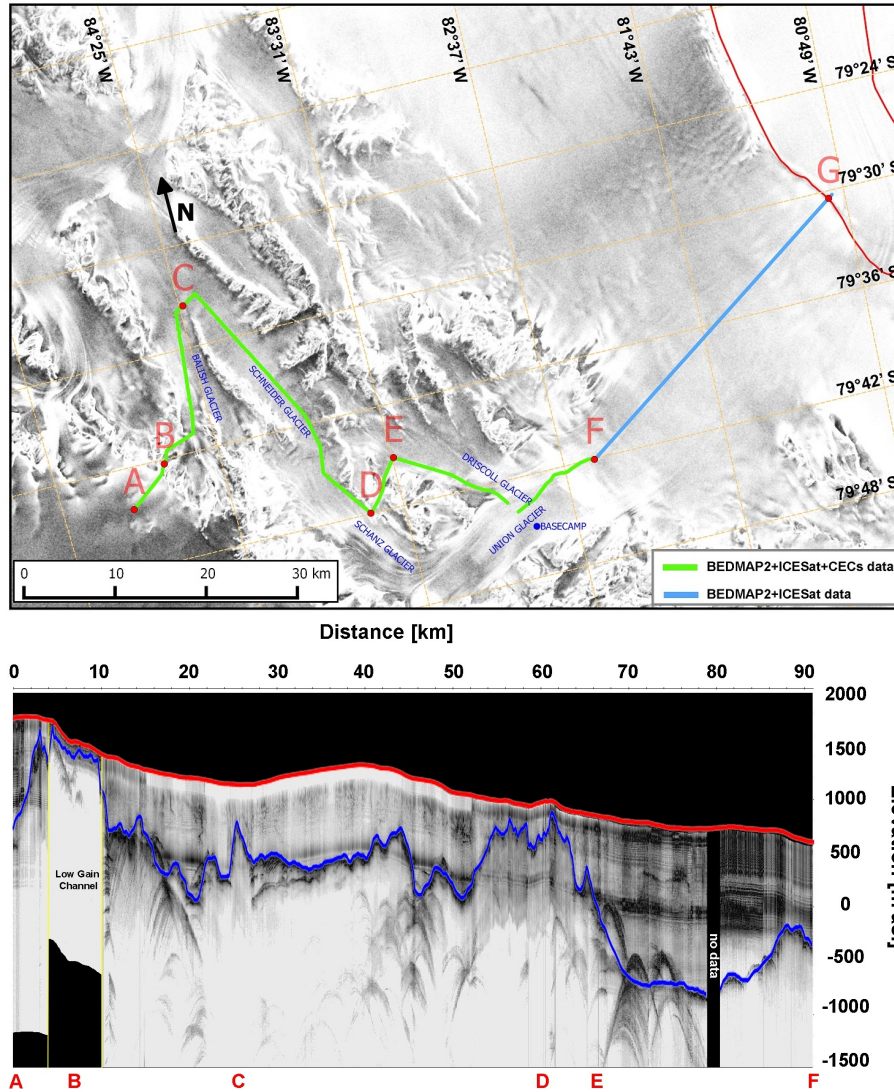


**Figure 6.** Upper: Location map of the radar and GPS survey measured between the Antarctic Plateau (A) and the Union Glacier (F) in 2010 (green line). In blue, the available data between F and the local Grounding Line Zone (in red, from Rignot et al. (2011a)) at the Constellation Inlet (G). The background image is the RAMP AMM-1 SAR Image Mosaic of Antarctica (Jezek and RAMP Product Team, 2002). Bottom: surface (red line) and subglacial topography (blue line) interpreted from the radar data collected in 2010 along the A-F track.

435 feeding Union Glacier from the upper Antarctic plateau. As  
 440 a result, the net mass balance at this BIA is negative, the  
 driving factor explaining the mass loses being sublimation  
 of ice during summer months, as no melting event has been  
 450 observed since 2007. However, melting events have been  
 observed in the region, especially at Patriot Hills, where a  
 small water pond was formed at the boundary between the  
 BIA and the nunatak during a very warm 1997 summer  
 (Carrasco et al., 2000).

445 In spite of this negative surface mass balance, the resulting  
 ice elevation changes between 2008-2011 at the Union gate  
 are very close to the error of the measurements (combined

error of 0.01 m), with a mean of  $-0.012 \text{ m a}^{-1}$  and high  
 spatial variability ( $\pm 0.044 \text{ m a}^{-1}$ ) among the gate stakes.  
 Accordingly, the glacier must be considered in equilibrium  
 without significant changes compared with previous data  
 (Rivera et al., 2010).

The ice velocities at the BIA fluctuate between 11 and  
 24  $\text{m a}^{-1}$  without significant changes between 2007 and  
 2011. However, downstream of the Union gate, the velocities  
 increase up to 33  $\text{m a}^{-1}$  at the continuous GPS stake (Bstat),  
 where no seasonal variations or tidal modulated variability  
 were detected.



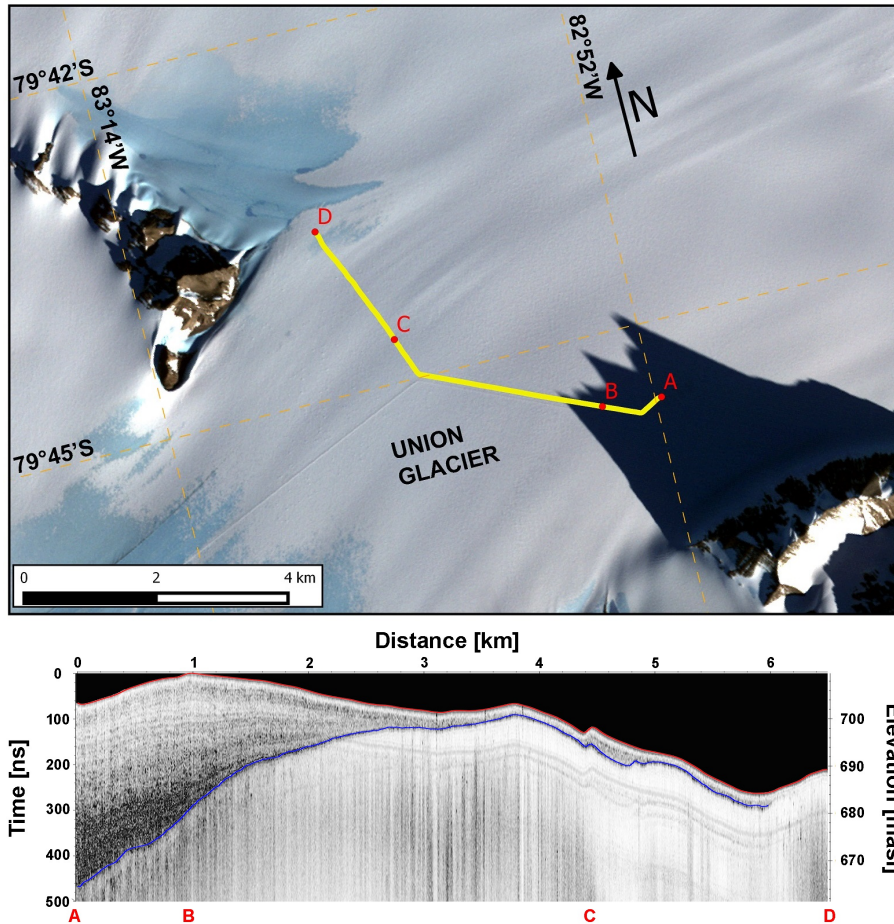


**Figure 7.** FM-CW data obtained at Union Glacier. Upper: location of the surveyed track near the base camp of Union Glacier. The background image is an ASTER false composite 321 acquired on 14 March 2013. Bottom: Radargram showing the surface topography (red line), internal annual snow/firn layers and the firm/ice boundary (blue line). Letters A and B indicate the base camp where the snow/firn layers are near 30-40 m thick in total. Letter C, corresponds to the medial moraine line of the glacier. Letter D, indicates the appearance of the BIA at the surface.

The GPR survey allowed the detection of many more crevasses than were previously mapped with the ASTER imagery (Rivera et al., 2014). The 400 MHz GPR is capable of identifying in real time surface and buried crevasses. The crevasses data were compared to the FM-CW records and in most of the cases the wider crevasses (2 to 4 m width) could be detected in both radars. However, the FM-CW radar did not provide the best information in regards to snow bridge thicknesses (less than 1 m), its resolution being insufficient to detect the first meters of the snow pack.

Comparisons of surface and bedrock topography along transect A – F (Fig. 8), resulted in a maximum ice thickness difference of 1447 m with a mean difference of 477 m (standard deviation: 348 m) between the data presented here and BEDMAP2 (Fretwell et al., 2013). The surface topography of the surveyed traverse was found to differ from BEDMAP2 and ICESat (2003-2005) by a mean of 91 m and

169 m, respectively. These differences are understandable due to the coarse resolution of BEDMAP2 and the footprint of ICESat.

The subglacial topography (Fig. 8) at the main trunk of the Union Glacier toward the local GLZ (Segment E-G in Fig. 6), showed a subglacial topography well below sea level (near -858 m), much deeper than previously estimated by BEDMAP2. However, between Union Glacier and the local GLZ, the subglacial topography shows a maximum altitude of -190 m at F in Figures 6 and 8. The subglacial topography then deepens toward the GLZ, where the bedrock is estimated to be 1050 m below sea level (Fretwell et al., 2013). This subglacial condition implies that an upstream migration of the GLZ until point F in Figures 6 and 8 will not have a strong effect on Union Glacier. However, the glacier can respond in a more dynamic way if this possible migration

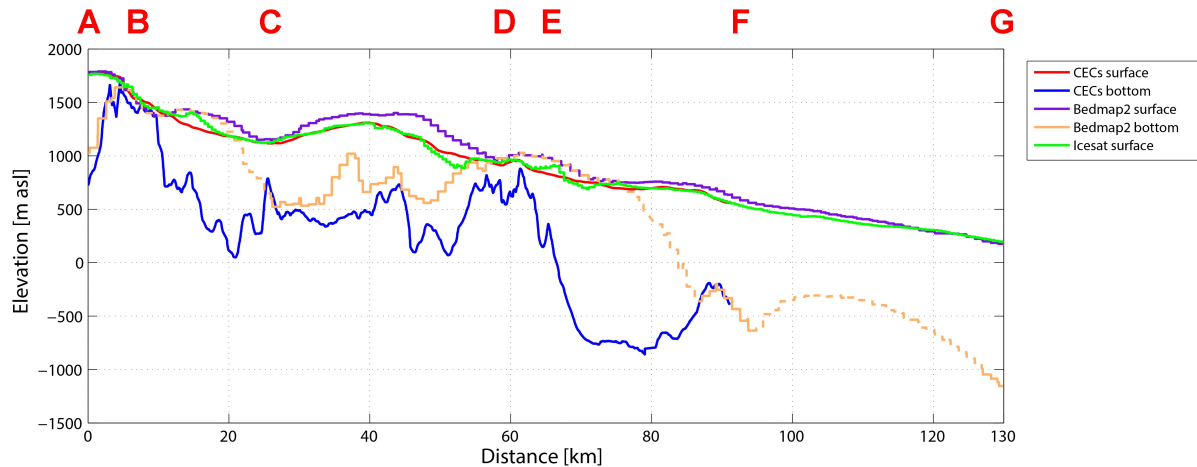


**Figure 8.** Comparisons of surface and bedrock topography of different data sources along transect A – G (see Fig. 6 upper for location of transect). CECs surface and bedrock from year 2010. ICESat surface from 2003–2005, BEDMAP2 surface and Bedrock from Fretwell et al. (2013). BEDMAP2 bottom dashed line is interpolated.

is affecting Union Glacier upstream this potential pinning point.

## 6 Conclusions

Several glaciological oversnow campaigns have been undertaken to Union Glacier and nearby areas since 2007, where the surface and subglacial topographies were mapped in detail. These results were compared to the BEDMAP2 dataset, showing much deeper bedrock and a much more complex subglacial topography. The obtained results determined a maximum ice thickness of 1540 m in Union Glacier, with a maximum snow ice boundary layer at 120 m. The internal structure of the ice was also mapped, including the detection of isochronous layers and crevasses, allowing logistic operators and scientists to work along safer routes.

Ice dynamics were also recorded thanks to the measurement of ice velocities and ice thickness. Maximum ice velocity values of  $34.6 \text{ m a}^{-1}$  were obtained. Near equilibrium conditions were calculated at the BIA, where mean velocities of  $20 \text{ m a}^{-1}$  were measured. The snow accumulation among the studied stakes outside BIAs showed values of up to  $0.2 \text{ m w.eq. a}^{-1}$  (near  $0.5 \text{ m a}^{-1}$  of snow). At the BIA, a local negative mass balance was detected as expected, with mean ablation rates of  $0.1 \text{ m w.eq. a}^{-1}$ .

Due to the below sea level subglacial topography upstream the local GLZ, it is expected that Union Glacier can experience some thinning and acceleration in future scenarios of GLZ migration. However these impacts will not affect the whole glacier, because at near 55 km upstream the present GLZ, the bedrock topography has a prominent

ridge perpendicular to the main ice flow direction, where the bedrock has a maximum altitude of  $-190 \text{ m asl}$ . This ridge can play an important role in modulating future glacier responses by enabling the grounding line to a prolonged stand-still, providing a “pinning point” to the glacier.

Overall the collected data allowed a ground route from Union Glacier to the upper Antarctic plateau to be satisfactory mapped. The route is important as it traverses the Subglacial lake Ellsworth and the main ice streams flowing into the Amundsen Sea Embayment area (Pine Island Glacier) and toward the Weddell Sea (Institute and Rutford Ice stream). This new 235 km long route toward Subglacial Lake Ellsworth is shorter than half of the previously traversed track of 517 km, providing a much direct and short gateway into inner Antarctica.

*Acknowledgements.* This research was supported by Antarctic Logistic Expeditions (ALE) Ltd. Special thanks to M. Sharp, M. and P. McDowell, C. Jacobs, Eddy, Boris and all ALE personnel at Union. CECs is funded by the Basal fund of CONICYT, among other grants. J. A. Neto collaborated with GPS data collection in 2011. A. Wendt, C. Rada, T. Kohoutek and M. Barandun helped with data processing. H. Gudmundsson analysed the GPS data at Bstat in order to detect possible tidal modulated effects on the ice flow. J. Carrasco and F. Burger helped with the met data. D. Carrión helped with figures and satellite image analysis. R. Wilson edited the text. A. Rivera is a Guggenheim fellow. The comments and suggestions by Ted Scambos and Neil Ross are highly appreciated.

## References

- Bamber, J., Riva, R., Vermeersen, B., and LeBrocq, A.:  
 550 Reassessment of the potential. Sea-level rise from a collapse of  
 the West Antarctic Ice Sheet Science, 324, 901–903,  
 2009. 610
- Brown, I. and Scambos, T.: Satellite monitoring of blue ice  
 extent near Byrd Glacier, Antarctica, *Annals of Glaciology*, 39,  
 555 223–230, 2005. 615
- Carrasco, J., Casassa, G., and Rivera, A.: A warm event at Patriot  
 Hills, Antarctica: An ENSO related phenomena?, in: Sixth  
 International Conference on Southern Hemisphere Meteorology  
 and Oceanography, pp. 240–241, Santiago, Chile, 2000.
- 560 Cavalieri, D. and Parkinson, C.: Antarctic sea ice variability  
 and trends, 1979–2006, *Journal of Geophysical Research*, 113,  
 doi:10.1029/2007JC004564, 2008. 620
- Conger, S. and McClung, D.: Comparison of density cutters for  
 snow profile observations, *Journal of Glaciology*, 55, 163–169,  
 565 2009. 625
- Fretwell, P., Pritchard, H., Vaughan, D., Bamber, J., Barrand, N.,  
 Bell, R., Bianchi, C., Bingham, R., Blankenship, D., Casassa,  
 G., Catania, G., Callens, D., Conway, H., Cook, A., Corr,  
 H., Damaske, D., Damm, V., Ferraccioli, F., Forsberg, R.,  
 570 Fujita, S., Gim, Y., Gogineni, P., Griggs, J., Hindmarsh, R.,  
 Holmlund, P., Holt, J., Jacobel, R., Jenkins, A., Jokat, W.,  
 Jordan, T., King, E., Kohler, J., Krabill, W., Riger-Kusk, M.,  
 Langley, K., Leitchenkov, G., Leuschen, C., Luyendyk, B.,  
 Matsuoka, K., Mouginot, J., Nitsche, F., Nogi, Y., Nost, O.,  
 575 Popov, S., Rignot, E., Rippin, D., Rivera, A., Roberts, J., Ross,  
 N., Siegert, M., Smith, A., Steinhage, D., Studinger, M., Sun,  
 B., Tinto, B., Welch, B., Wilson, D., Young, D., Xiangbin, C.,  
 and Zirizzotti, A.: Bedmap2: improved ice bed, surface and  
 thickness datasets for Antarctica, *The Cryosphere*, 7, 375–393,  
 580 doi:10.5194/tc-7-375-2013, 2013. 640
- Glen, J. and Paren, J.: The electrical properties of snow and ice,  
*Journal of Glaciology*, 15, 15–38, 1975.
- Gudmundsson, G.: Fortnightly variations in the flow velocity of  
 Rutford Ice Stream, West Antarctica, *Nature*, 444, 1063–1064,  
 585 2006. 645
- Hellmer, H., Kauker, F., Timmermann, R., Determann, J., and Rae,  
 J.: Twenty – first – century warming of a large Antarctic ice-shelf  
 cavity by a redirected coastal current, *Nature*, 485, 225–228,  
 2012.
- 590 Hooke, R.: Principles of Glacier Mechanics, Cambridge University  
 Press, Cambridge, UK, second edn., 2005.
- Jezeq, K. and RAMP Product Team: RAMP AMM-1 SAR Image  
 Mosaic of Antarctica. Version 2. Fairbanks, AK: Alaska Satellite  
 Facility, in association with the National Snow and Ice Data  
 595 Center, Boulder, CO. Digital media, 2002. 655
- Joughin, I. and Bamber, J.: Thickening of the ice stream catchments  
 feeding the Filchner-Ronne Ice Shelf, Antarctica, *Geophysical  
 Research Letters*, 32, L17503, doi:10.1029/2005GL023844,  
 2005.
- 600 Mayewski, P., Meredith, M., Summerhayes, C., Turner, J., Worby,  
 A., Barrett, P., Casassa, G., Bertler, N., Bracegirdle, T., Naveira,  
 A., Bromwich, D., Campbell, H., Hamilton, G., Lyons, W.,  
 Maasch, K., Aoki, S., Xiao, C., and van Ommen, T.: State of  
 the Antarctic and Southern Ocean climate system, *Review of  
 605 Geophysics*, 47, RG1003, doi:10.1029/2007RG000231, 2009.
- Paterson, W.: The physics of glaciers, Pergamon Press, Great  
 Britain, 3rd edn., 1994.
- Plewes, A. and Hubbard, B.: A review of the use of radio-echo  
 sounding in glaciology, *Progress in Physical Geography*, 25,  
 203–236, 2001.
- Rignot, E. and Jacobs, S.: Rapid bottom melting widespread near  
 Antarctic Ice Sheet grounding lines, *Science*, 296, 2020–2023,  
 2002.
- Rignot, E. and Thomas, R.: Mass balance of polar ice sheets,  
*Science*, 297, 1502–1506, 2002.
- Rignot, E., Vaughan, D., Schmelz, M., Dupont, T., and MacAyeal,  
 D.: Acceleration of Pine Island and Thwaites Glaciers, West  
 Antarctica, *Annals of Glaciology*, 34, 189–194, 2002.
- Rignot, E., Mouginot, J., and Scheuchl, B.: Antarctic  
 grounding line mapping from differential satellite radar  
 interferometry, *Geophysical Research Letters*, 38, L10504,  
 doi:10.1029/2011GL047109, 2011a.
- Rignot, E., Mouginot, J., and Scheuchl, B.: Ice Flow of the Antarctic  
 Ice Sheet, *Science*, 333, 1427–1430, 2011b.
- Rivera, A., Zamora, R., Rada, C., Walton, J., and Proctor,  
 S.: Glaciological investigations on Union Glacier, Ellsworth  
 Mountains, West Antarctica, *Annals of Glaciology*, 51, 91–96,  
 2010.
- Rivera, A., Cawkwell, F., Wendt, A., and Zamora, R.: Mapping  
 Blue Ice Areas and Crevasses in West Antarctica Using ASTER  
 Images, GPS and Radar Measurements, in: *Global Land Ice  
 Measurements from Space*, edited by Kargel, J., Leonard, G.,  
 Bishop, M., Kääh, A., and Raup, B., chap. 31, pp. 743–757,  
 Springer-Praxis, Heidelberg, 2014.
- Ross, N., Bingham, Corr, H., Ferraccioli, F., Jordan, T., Le Brocq,  
 A., Rippin, D., Young, D., Blankenship, D., and Siegert, J.: Steep  
 reverse bed slope at the grounding line of the Weddell Sea sector  
 in West Antarctica, *Nature Geosciences*, 5, 393–396, 2012.
- Scambos, T., Haran, T., Fahnestock, M., Painter, T., and Bohlander,  
 J.: MODIS-based Mosaic of Antarctica (MOA) data sets:  
 continent-wide surface morphology and snow grain size, *Remote  
 Sensing of Environment*, 111, 242–257, 2007.
- Uribe, J., Zamora, R., Gacitúa, G., Rivera, A., and Ulloa, D.: A low  
 power consumption radar system for measuring ice thickness and  
 snow/firn accumulation in Antarctica, *Annals of Glaciology*, 55,  
 39–48, 2014.
- Vaughan, D., Rivera, A., Woodward, J., Corr, H., Wendt,  
 J., and Zamora, R.: Topographic and hydrological controls  
 on Subglacial Lake Ellsworth, West Antarctica, *Geophysical  
 Research Letters*, 34, L18501, 2007.
- Wendt, A., Casassa, G., Rivera, A., and Wendt, J.: Reassessment  
 of ice mass balance at Horseshoe Valley, Antarctica, *Antarctic  
 Science*, 21, 505–513, 2009.
- Woodward, J. and King, E.: Radar surveys of the Rutford Ice Stream  
 onset zone, West Antarctica: indications of flow (in)stability?,  
*Annals of Glaciology*, 50, 57–62, 2009.

**Table 1.** BIA extension based upon ASTER images collected since 2002.

Year/month/day	Area (km <sup>2</sup> )
2002/11/24	95.6
2004/12/09	104.7
2007/01/27	112.0
2009/01/17	111.8
2012/02/11	88.2
2013/02/01	96.7

**Table 2.** Stake co-ordinates, velocities and mass balance per period. See Figs. 1 and 2 for locations.

Stakes	Lat°	Lon°	H. (m.a.e)	Velocity (m/a)	Mass Balance (m w.eq./a)	Period	Type of surface	
B1	-80.211	-81.230	803.12	12.7	0.18	2008-2009	snow	
B2	-80.124	-81.113	813.51	1.8	0.19			
B3	-80.045	-80.937	759.07	0.6	0.04			
B4	-79.985	-81.080	573.57	1.8	0.06		2008-2009	snow/BIA
B5	-79.922	-81.211	538.16	2.0	-0.07			
B6	-79.840	-81.298	669.59	0.1	0.03			
B7	-79.801	-81.348	553.87	1.2	0.04			
B8	-79.757	-81.965	459.99	2.9	0.14			
B9	-79.709	-82.455	531.04	33.3	0.14			
Bstat	-79.708	-82.454	531.34	33.0	-	2009/11/12 2010/31/01	snow	
B10	-79.717	-82.643	639.79	34.6	0.17	2008-2009	ice	
B11	-79.757	-82.803	672.46	20.5	0.13			
B12	-79.760	-82.931	690.56	20.9	0.20			
B13	-79.764	-83.091	703.53	22.9	-0.09			
B14	-79.768	-83.266	738.39	22.4	-0.06			
B15	-79.798	-83.281	735.19	21.6	-0.16			
B16	-79.796	-83.316	742.20	23.2	-0.13			
B17	-79.765	-83.343	739.36	17.0	-0.08		ice/crevasses	
B18	-79.760	-83.370	747.68	14.0	-0.11			
B19	-79.764	-83.372	743.72	11.1	-0.10			
V00	-79.769	-83.370	739.47	18.1	-0.08	2008-2010	ice	
V01	-79.770	-83.370	738.44	19.0	-0.08	2007-2011		
V02	-79.772	-83.368	738.13	20.2	-0.04	2007-2010		
V03	-79.774	-83.365	739.69	21.7	-0.11	2007-2011		
V04	-79.775	-83.363	736.40	22.3	-0.07			
V05	-79.777	-83.361	733.57	23.0	-0.22			
V06	-79.779	-83.358	735.12	23.5	-0.11	2007-2010		
V07	-79.781	-83.355	736.61	23.9	-0.08	2007-2009		
V08	-79.784	-83.352	739.05	24.3	-0.13			
V09	-79.787	-83.343	738.60	24.3	-0.11			
V10	-79.790	-83.334	737.63	24.3	-0.13	2007-2011		
V11	-79.792	-83.325	738.82	24.0	-0.07	2007-2010		
V12	-79.771	-83.337	738.51	21.9	-0.09	2007-2011		
V13	-79.773	-83.335	735.87	22.3	-0.08			
V14	-79.774	-83.332	733.20	22.4	-0.08			
V15	-79.777	-83.327	731.27	22.7	-0.09			
V16	-79.779	-83.323	731.72	23.1	-0.10			
V17	-79.782	-83.316	731.16	23.4	-0.11	2007-2011		
V18	-79.784	-83.313	730.33	23.5	-0.13			
V19	-79.786	-83.309	729.48	23.6	-0.07			
V20	-79.788	-83.303	728.57	23.3	-0.11			
V21	-79.791	-83.298	733.66	23.0	-0.07			